Global implications of 1.5 °C and 2 °C warmer worlds on extreme river flows

Environmental Research Letters

LETTER

Global implications of 1.5 °C and 2 °C warmer worlds on extreme river flows

Homero Paltan[1,2], **Myles Allen**[3], **Karsten Haustein**[3], **Lena Fuldauer**[3] **and Simon Dadson**[1]

[1] School of Geography and the Environment, University of Oxford, Oxford, United Kingdom
[2] Instituto de Geografia, Universidad San Francisco de Quito, Quito, Ecuador
[3] Environmental Change Institute, University of Oxford, Oxford, United Kingdom

E-mail: homero.paltanlopez@ouce.ox.ac.uk

Keywords: Paris Agreement, high flows, climate change

Supplementary material for this article is available online

OPEN ACCESS

RECEIVED
23 November 2017

REVISED
9 July 2018

ACCEPTED FOR PUBLICATION
10 August 2018

PUBLISHED
24 August 2018

Abstract

Targets agreed to in Paris in 2015 aim to limit global warming to 'well below 2 °C and to pursue efforts to limit the temperature increase to 1.5 °C above pre-industrial levels'. Despite the far-reaching consequences of this multi-lateral climate change mitigation strategy, the implications for global river flows remain unclear. Here we estimate the impacts of 1.5 °C versus 2.0 °C mitigation scenarios on peak flows by using daily river flow data from a multi-model ensemble which follows the HAPPI Protocol (that is specifically designed to simulate these temperature targets). We find agreement between models with regard to changing risk of river flow extremes. Moreover, we find that the response at 2.0 °C is not a uniform extension of the response at 1.5°, suggesting a non-linear global response of peak flows to the two mitigation levels. Yet committing to the 2.0 °C warming target, rather than 1.5 °C, is projected to lead to an increase in the frequency of occurrence of extreme flows in several large catchments. In the most affected areas, predominantly in South Asia, while region-specific features such as aerosol loads may determine precipitation patterns, we estimate that under our 1.5 °C scenario the historical 1-in-100 year flow occurs with a frequency of 1-in-25 years. At 2.0 °C, similar increases are observed in several global regions. These shifts are also accompanied by changes in the duration of rainy seasons which influence the occurrence of high flows.

1. Introduction

The Conference of the Parties of the United Nations Framework Convention on Climate Change (UNFCCC) in its Paris Agreement in December 2015 agreed to hold 'the increase in the global average temperature to well below 2 °C above pre- industrial levels and to pursue efforts to limit the temperature increase to 1.5 °C above pre-industrial levels'. The simplicity of these targets led parties to the treaty to embrace a common climate strategy with the aim of preventing the risks and impacts associated with unabated climate change (Hulme 2016, Rogelj *et al* 2016, Schellnhuber *et al* 2016).

Yet the assumption that a 2 °C limit is a safe bar as far as climate-change related tipping points are concerned, has diverted attention away from the difference in impacts between worlds in which global temperatures are stabilized at 1.5 °C instead of 2.0 °C. Overlooking these thresholds may have important consequences given the sensitivity of high flows to radiative forcings (Milly *et al* 2002). In particular, early studies projected an increase in annual runoff and flow peaks in snow-dominated catchments as a result of climate change (Nijssen *et al* 2001). From here, several studies have projected increases in high flow and flood frequency in Southeast Asia and eastern Africa, although important shifts have also been calculated for other regions such as the northern Andes, North America, and eastern Europe (Okazaki 2012, Hirabayashi *et al* 2013, Dankers *et al* 2014, Koirala *et al* 2014). As such, the impacts of extreme river flows on human lives, socio-economic development, and monetary losses may be particularly important in a changing climate

(Peduzzi *et al* 2009, Wake 2013, Arnell and Lloyd-Hughes 2014, Jongman *et al* 2014, Winsemius *et al* 2015, Arnell and Gosling 2016).

More recently, by downscaling climate projections and finding the corresponding year in which various levels of atmospheric warming are exceeded, a positive increase in future flood risk has been projected (Alfieri *et al* 2017). While the future increment in flood risks is important when compared to its historical baseline, the impacts appear to be more important at 4.0 °C if compared to the less evident shifts observed between 1.5 °C and 2.0 °C.

Yet, since climatological biases in current climate models experiments, such as the Coupled Model Intercomparison Project, remain of the order of 0.5 °C these efforts may not be sufficient to differentiate the risk associated with these two levels of warming (Hulme 2016, Mitchell *et al* 2016). For the hydrological cycle, in particular, the distribution of global precipitation between CMIP scenario experiments does not respond uniformly between CMIP scenario experiments due to the changing role of non-CO_2 forcing over the 21st century and also due to the precipitation sensitivity to emission-scenarios. This, in turn, makes it difficult to differentiate whether detected differences result from additional warming or additional factors. So, extracting anomalies for 1.5 °C and 2.0 °C levels of warming from the traditional CMIP scenarios driven experiments may not be scientifically robust (Mitchell *et al* 2016).

With such concerns in mind, the HAPPI protocol was specifically designed to simulate the specified Paris Agreement temperature targets (1.5 °C and 2.0 °C) as precisely as possible by separating the impact of an additional approximately half degree of warming from uncertainty in climate model responses and internal climate variability (Mitchell *et al* 2017). So, unlike other multi-model exercises, HAPPI does not exclusively rely on prescribed radiative forcing protocols to project the future temperature evolution, but robustly constrains it using prescribed future sea surface temperatures (SSTs) as well. This effectively reduces the influence of model sensitivity and results in a narrowly defined range of future temperature targets. Thus, the HAPPI Protocol provides an improved framework for the analysis of the impacts of an additional half degree of warming.

In this study, we estimate the extent to which global peak river flows seen under a 1.5 °C scenario differ from those under a 2 °C scenario. In particular, we investigate where shifts in high flow occurrence would be more important under these climate scenarios. We follow the HAPPI experimental protocol, to use the multi-model-ensemble daily output of four atmosphere-only general circulation models (AGCMs). Total runoff values were used to drive a river-flow routing scheme to calculate daily river flows for the: (a) present baseline (2006–2015), (b) 1.5 °C scenario, and (c) 2 °C scenario. From here we compute river flow extreme statistics to calculate changes in high flow occurrence and magnitude.

2. Methods

2.1. HAPPI experiments and data

The HAPPI protocol provides three 10 year simulation periods with prescribed atmospheric forcing, sea-surface temperature and sea-ice coverage. The three scenarios are: (1) the reference or historical period which is the 'current decade' from 2006 to 2015, (2) a future decade that is about 1.5 °C warmer than pre-industrial levels, and (3) a future decade that is about 2.0 °C warmer than pre-industrial levels. In this protocol, the reference experiment chosen is 2006–2015 because it is the most recently observed period. This period also contains a range of different SST patterns over the decade, allowing for an assessment of how the ocean conditions vary on inter-annual timescales, including important El Niño and La Niña events.

For each scenario, we used the output of four HAPPI AGCMS: CanAM4 (100 ensemble members); CAM4-2degree (100 ensemble members); NorESM1-HAPPI (125 ensemble members), and MIROC5 (50 ensemble members). Each simulation (ensemble member) within an experiment differs from the others in its initial weather state. So, the use of 50–125 ten-year time slices really provides 500 years of data for the MIROC5 experiment, 1000 years for CanAM4 and CAM4-2degree; and 1250 years for NorESM1-HAPPI. Such extensive record (500–1250 years) in turn provides the basis for robust calculations. More details of the HAPPI protocol is found in the supplementary information is available online at stacks.iop.org/ERL/13/094003/mmedia.

2.2. Runoff

The AGCMs used in this study have a land surface scheme which is coupled to the overlying atmosphere. For two models, NCC/NorESM1-HAPPI and ETH/CAM4-2degree, runoff was stored in the HAPPI archive. The other two models (MIROC/MIROC5 and CCCma/CanAM4) did not have a runoff-production scheme activated for use in the present experiment and so we applied a comparable runoff-generation scheme to calculate runoff in those cases. This in turn enabled us to use those models alongside the members of the ensemble for which runoff data were available.

So, for these two AGCMs we calculated runoff by using a simple runoff production model designed to be comparable with the runoff-production models typically embedded within climate models. Our scheme uses a Rutter–Gash canopy formulation (Gash 1979) together with Penman–Monteith evaporation calculated using available radiation data (Monteith 1965). Soil moisture was accounted for

using a two-layer model with saturation-excess runoff computed using a generalized TOPMODEL (Clark and Gedney 2008).

The snowpack model used here was based on a temperature-based model of accumulation and melt (Moore *et al* 1999, Hock 2003, Beven 2011). Snow accumulates when precipitation falls while temperature is below a threshold temperature T_a. When temperature is above a threshold for melt, T_m melting occurs at a rate proportional to the difference between the current temperature and T_m. This conceptual model is widely used (Hock 2003, Zhang *et al* 2006, Rango and Martinec 2007, Beven 2011) and gives performance comparable with that of more parameter-rich energy balance models, despite their greater complexity (Parajka *et al* 2010).

We acknowledge the existence of other more sophisticated runoff schemes yet ours is intended to be applied directly to atmospheric outputs resulted from large ensembles such as the HAPPI ensemble allowing us to maximize the utility of the HAPPI ensemble by generating runoff when it was not provided directly. Comparison of our simulated runoff indicates good latitudinal agreement with observations provided by the World Meteorological Organization Global Runoff Data Center (GRDC) (Fekete *et al* 2002) (see supplementary figure 4).

2.3. Runoff routing

Total runoff derived from NCC/NorESM1-HAPPI and ETH/CAM4 models or calculated from CCCma/CanAM4 and MIROC/MIROC5 were routed by implementing the grid-based hydrological routing scheme as presented by Dadson *et al* (2011). This scheme is based on the discrete approximation to the 1D kinematic wave equation with lateral inflow (Oki and Sud 1998). This routing model routes flows along the path of steepest descent. Resistance to flow is handled via a wave celerity parameter. This algorithm has been widely used in various large-scale hydrological studies as well as various existing climate and land surface model configurations. Further details are available in Bell *et al* (2007). We also selected this scheme as it is computationally tractable when dealing with a global problem with many hundreds of ensemble members, as with the HAPPI experiment.

Also, in this scheme the river network data used was constructed by using the network tracing method (NTM) which is a vector-based network scheme that traces the path of river networks downstream (Olivera and Raina 2003). This method works by overlaying a mesh of a certain grid size over a fine-scale joined river network to determine the coarse-scale downstream cell. This method has the advantage that it can be used in areas where digitized river networks exist but no DTM is available and it is usually spatially closer to the base river network. As NTM has been found to outperform other raster-based methods, it has been widely used in previous routing studies (Olivera and Raina 2003, Bell *et al* 2007, Davies and Bell 2009). The resolution of the river network used here is half degree (0.5° × 0.5°).

Also, the spatial resolution of runoffs given by each AGCM (NCC/NorESM1-HAPPI: 1.875° × 0.625°; ETH/CAM4: 2.5° × 1.875°, MIROC/MIROC5: 1.40° × 1.40°, CCCma/CanAM4: 2.81° × 2.81°) was downscaled to match the resolution of our river network. The downscaling was performed by applying a bilinear interpolation technique. Apart from its simplicity, this technique has been found to provide a more realistic spatial gradient instead of patches of same runoff values from an AGCM in cells with finer resolution (Koirala *et al* 2014); as consequence this method has been used in a range of global hydrological studies (Qian *et al* 2006, Materia *et al* 2009, Ukkola and Prentice 2013, Koirala *et al* 2014).

The final results of our study are presented at the scale of the routing model (0.5° × 0.5°). We acknowledge that this increase in the spatial representation of runoff may result in our overlooking or underrepresenting runoff processes that operate at finer scales, which are represented by using statistical distributions of sub-grid runoff generation. We note that our routing scheme does not account for human interventions and flow regulations such as dams and reservoirs, or changes in land use and river interventions. We acknowledge the importance of these anthropogenic interventions, but they are not the subject of our study. Models that incorporate complex anthropogenic processes do not typically offer computational simplicity appropriate for use with large ensembles. The comparison of derived river flows with observations derived from GRDC can be found in supplementary figure 5.

2.4. River flow extreme statistics

The change in high flow hazards between the historical and future conditions (1.5 °C and 2 °C warming scenarios) was calculated from the probability of the historical 100 year return period river flow magnitude to be exceeded at the 1.5 °C and 2 °C warming scenarios. We selected the 100 year return period as the reference river flow in order to keep consistency with previous hydrological studies (Dankers and Feyen 2008, Hirabayashi *et al* 2008, Ward *et al* 2013). So, time series (500–1250 years) of simulated annual maximum daily river flows in the historical scenario (2006–2015) were fitted to a two-parameter Gumbel distribution (Gumbel 1941). As a result, the magnitude of the 100 year return period river flow of the historical scenario was calculated at each grid and for each AGCM. Lastly, the return period of the historical 100 year river flow was calculated for the time series of the 1.5 °C and 2 °C warming scenarios.

A two-parameter Gumbel distribution was selected as it provides relatively stable distribution

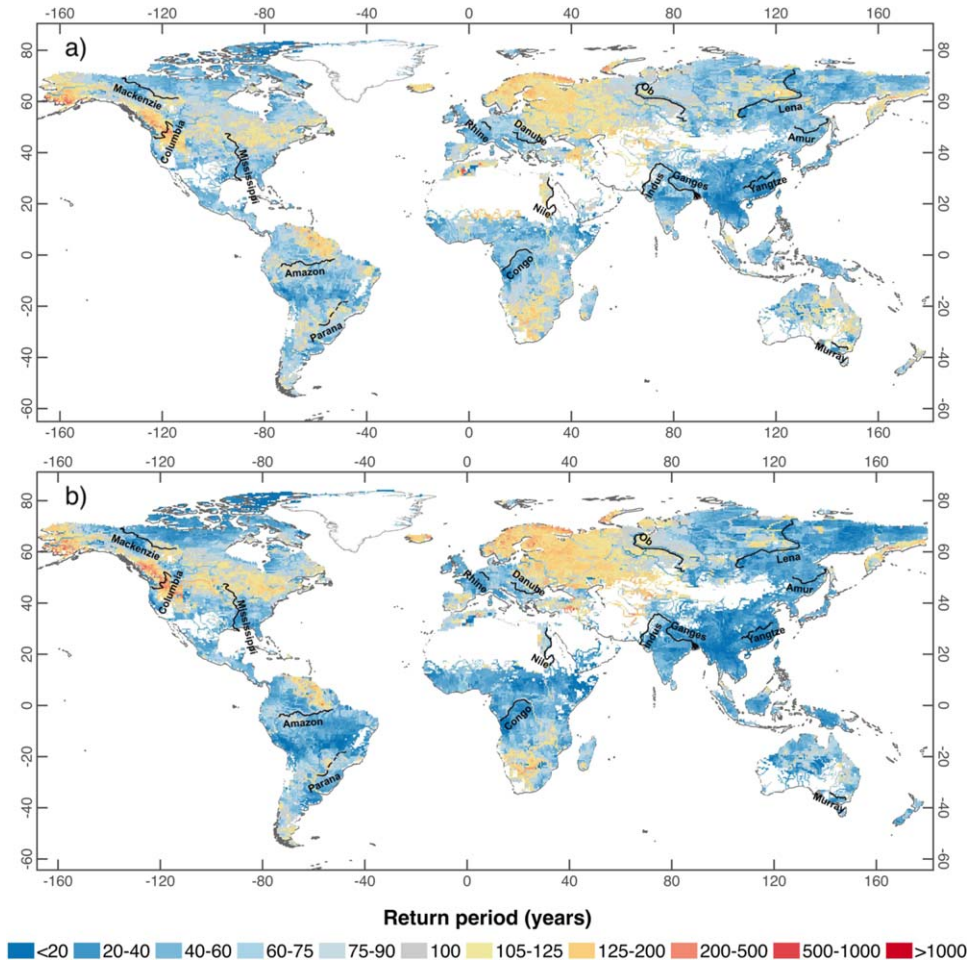

Figure 1. Multi-model median return period (years) for future river flow corresponding to the historical 100 year flow under (a) at 1.5 °C scenario (b) at 2 °C scenario. Grid boxes where the historical averaged annual flow is <10 m^3 s^{-1} were screened out. Blue colors indicate a more frequent historical 100 year flow whereas red colors indicate a reduction in the frequency.

parameters showing adequate results in similar previous studies (Hosking and Wallis 2005, Dankers and Feyen 2008, Hirabayashi *et al* 2008, Hirabayashi *et al* 2013). Also, while these previous studies acknowledge that the type of extreme distribution function selected may impact the probabilities of extreme flows, it does not affect the estimation changes in the frequency and tendency of them, which is the aim of this study. Similarly, Hirabayashi *et al* (2013) used the probability plot correlation coefficient test to find that globally 76% of the AGCMs adequately fit to the Gumbel distribution (coefficient > 0.96 at 95% of significance). Grids that did not fit this distribution were mostly found in arid regions which has also been found in similar studies (Hirabayashi *et al* 2008).

3. Results

We detect regions where the shift in occurrence of global historical extreme flows at 1.5 °C and at 2.0 °C differ as calculated by our ensemble of four AGCMs (figure 1). First, we identify regions that show an initial increase in the frequency of occurrence of historical high flows at 1.5 °C and then progressively increases at 2.0 °C. These regions include South America (Amazon catchment), central Africa, central-western Europe, the south of the US (Mississippi river area), central Asia, and Siberian catchments. In these regions, the median increase of the frequency of the current 1-in-100 year flow is once in 70–90 years at 1.5 °C, and at 2.0 °C this frequency increases to at least once in 50 years. Moreover, we find that in most of central and eastern China, the southern part of the Amazon catchment, the Blue Nile, and in northern India, the 1-in-100 year flow at 1.5 °C ranges between 1-in-50 and 1-in-60 years, whereas at 2 °C such an event ranges between 1-in-25 and 1-in-35 years.

Second, we identify areas where the frequency of the 1-in-100 year flow increases at 1.5 °C but does not change appreciably between 1.5 °C and 2.0 °C. Notably these areas are located in South and Southeast Asia (south of the Yangtze river) and the Indus river basin. In these regions under a 1.5 °C scenario, the current 1-in-100 year flow increases in frequency to 1-in-50 year return period. However, we also identify some areas, such as Southeast Asia, where the current 100 year flood occurs 1-in-25 years in the future. In North

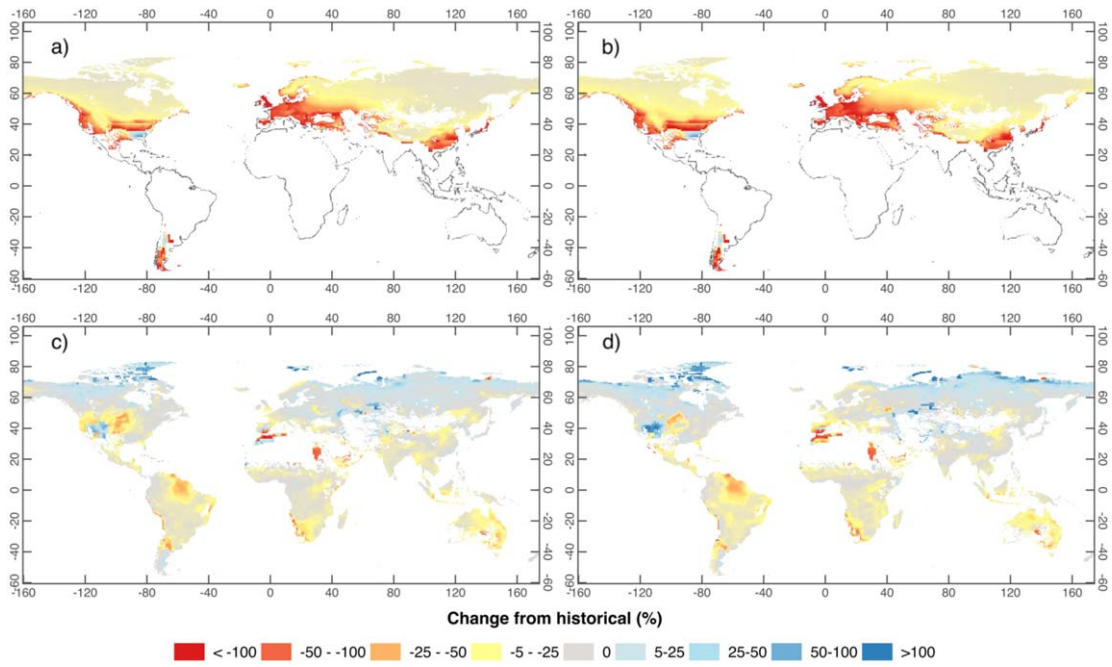

Figure 2. Multi-model median change (%) in the number of frost days between the historical and: (a) 1.5 °C scenario, (b) 2.0 °C scenario. A frost day is that where estimated temperatures are less than 0 °C. (c) and (b) is as (a) and (b), correspondingly, but for the number of days with precipitation. We define a day with precipitation as that where estimated daily precipitation is greater than 2 mm d^{-1}. This threshold is selected as it adequately describes the range of global *light* precipitation (0.1–5 mm d^{-1}) (Qiaohong *et al* 2017).

America and eastern Europe, the current 100 year return period flow increases in frequency only slightly, to once in 80 years at 1.5 °C.

We also find some regions which see a decrease in the frequency of high flows between the present day and 1.5 °C or 2.0 °C or both. These regions are located in the northern part of South America, areas of the western coast of the United States (Colorado River) and Canada, South Africa (Orange River), Scandinavia, and in some parts of eastern Europe. In most of these regions, we note that the current 1-in-100 year flow decreases in frequency to approximately 1-in-150 years, with little further decrease at 2.0 °C. Lastly, we find that in the area of the Murray-Darling basin in Australia, there is a shift from historical high flows not changing in a world 1.5 °C warmer (projected return periods between 90 and 125 years), whilst under a 2.0 °C scenario the return period decreases to approximately 1-in-70 years.

3.1. Physical characterization of high flows

In order to understand the physical reasons that induced shifts in high flow frequencies, we calculated the change in both the number of frost days and the number of days where precipitation has occurred between the two scenarios in comparison to the historical baseline (see figure 2). We find an important decrease in the number of frost days at 1.5 °C which slightly increases at 2.0 °C. This decrease is greater in North America, and central and eastern Europe (figures 2(a), (b)). This finding suggests that globally the role of snowmelt in the generation of high flows will decrease as snow accumulation reduces. Exceptions to this pattern are found in the South and East Coast of the US and in the south of South America. In these areas, particularly in the US, where we estimate an increase in the occurrence of high flows, snow dynamics and possibly longer periods of snow accumulation may be important drivers of high flow events.

The change in the number of days with precipitation between the two climate thresholds (figures 2(c), (d)) shows a diverse regional response. For example, in most of the regions where we estimate a progressive increase in the frequency of high flows between 1.5 °C and 2.0 °C, such as central-western Europe or South America, the number of days with precipitation typically decreases or does not importantly change at 1.5 °C and also at 2.0 °C. This is also accompanied by a decrease in average annual precipitation magnitudes at both scenarios (see supplementary figure 2). This result suggests that in these areas extreme precipitation, will likely dominate the occurrence of high flows, despite the reduction in the number of rain days. An important exception is observed in Siberia, where we see an increase in the frequency of high flows accompanied by a slight decrease in the number of days with precipitation.

In regions where the increase in high flow occurrences is important at 1.5 °C but minor at 2.0 °C, such as the south of Asia, we find that, at this first temperature target, the frequency of rain days decreases as

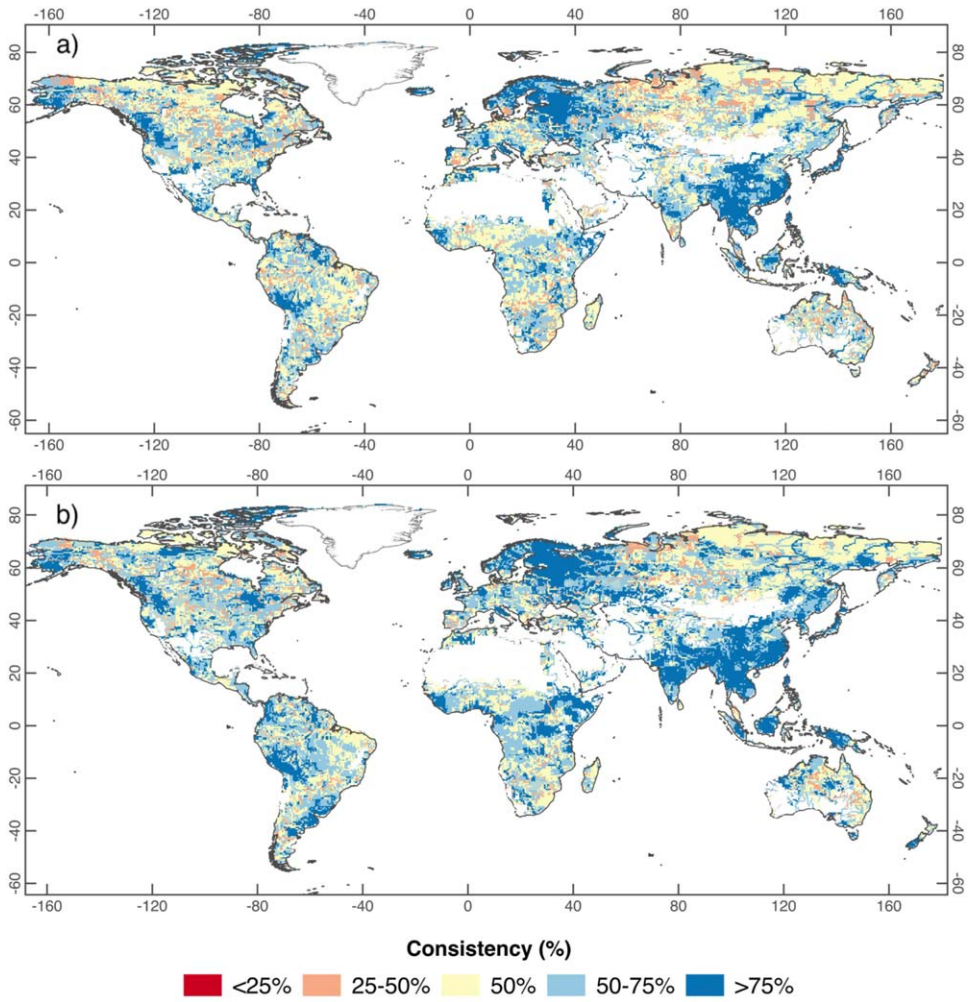

Figure 3. Consistency in projected river flow change for the four AGCMs used in this study. Consistency is expressed as a percentage of the total the number of models that agree with the tendency in the direction of change (increase or decrease) of the historical return period.

well as total annual precipitation magnitudes. Yet at 2.0 °C days with precipitation are either more common (especially in North America) or show a lower reduction compared with that detected at 1.5 °C. Similarly, annual precipitation magnitudes show a slight increase when compared to the historical reference period. This finding suggests that, in these regions, the role of shorter wet seasons and storms in high flows, which at 1.5 °C seems to be more important, will decrease at 2.0 °C. So, in these regions, the difference between the two climate targets, and thus flow occurrences, may be associated with shifts in durations and characteristics of the wet season. In the regions where we observe a decrease in the occurrence of high flows, we also detect a decrease in the number of days with precipitation and annual precipitation magnitudes.

3.2. Multi-model consistency and biases in results

The change in high flow frequency at 1.5 °C and 2.0 °C, although consistent in sign between models across most parts of the globe, differs in specific regions (see figure 3). Globally, we find that 49% of land grid cells at 1.5 °C and 43% at 2.0 °C show a high consistency in the tendencies described above (consistency defined as an agreement in trajectory of three out of four models). This high level of consistency is seen particularly in regions where we find an increase in high flow frequency, such as the south of Asia, India, or East Africa. Conversely, in just about 7% of land grid cell at 1.5 °C and 4% at 2.0 °C just one model agrees with the tendency mapped above. Typical regions with lower consistencies can be found in northern Russia and parts of the tropics. In these areas our projections are subject to an important spread across the AGCM ensemble.

Additionally, the examination of the way each AGCM simulates the changes in high frequency helps to disseminate further model biases (supplementary figure 1). For instance, NCC/NorESM1-HAPPI generally projects greater increases in the frequency of occurrence of the reference high flow in the tropics. Thus, it simulates a more pronounced increase in high flow from the historical reference return time of 1-in-100 years to approximately 1-in-40 years at 2.0 °C for

Table 1. Projected change (expressed as return period) of the 1-in-100 year historical flow at both scenarios and estimated change in the mean river flow (%) from ten selected major global outlets. Uncertainty due to sample size is calculated by a bootstrap method. Uncertainty for the four AGCMs was averaged. Standard deviation is calculated from our ensemble of AGCMs.

	Return period of historical high flow				Change in mean historical river flow (%)			
	1.5 °C		2.0 °C		1.5 °C		2.0 °C	
River system	R. period (year)	Uncertainty due to sample size	R. period (year)	Uncertainty due to sample size	Mean	Std	Mean	Std
Amazon	108	±5	87	±3	−4.7	1.3	−5.2	2.6
Mississipi	85	±3	64	±4	1.0	2.4	1.6	5.1
Mackenzie	61	±7	49	±4	6.3	2.4	8.9	3.7
Congo	80	±6	57	±5	−0.6	2.2	−0.2	4.2
Nile	92	±7	55	±4	−1.2	2.2	2.8	3.4
Rhine	70	±8	72	±7	2.6	2.4	1.3	3.2
Danube	54	±8	63	±6	2.0	5.4	−1.8	5.1
Murray-Darling	143	±5	96	±5	−9.0	1.7	−4.0	4.8
Ganges	67	±4	41	±3	1.7	3.6	5.0	4.7
Indus	130	±6	127	±6	−1.2	5.1	−0.3	7.4
Yangtze	58	±8	26	±9	7.4	4.9	8.2	5.9
Ob'	54	±9	48	±9	5.7	3.2	7.5	5.1

larger areas (e.g., central South America and South Asia). Also, MIROC/MIROC5 and CCCma/CanAM4 show greater increases in reference extreme flow frequencies in northern regions. We also find that ETH/CAM4-2degree generally produces lower river flows outside the tropics.

Moreover, by examining the way each AGCM represents precipitation and then runoff (supplementary figure 3 for precipitation and 4 for runoff), we estimate whether existing biases (such as the lower river flow in ETH/CAM4-2degree) are due to deficiencies in the AGCM, runoff generated, or the river routing model. Using zonal means, we find that each of the four AGCMs slightly overestimates mean precipitation in the tropics compared with the Global Precipitation Climatology Center dataset, GPCC (Becker *et al* 2011) (maximum precipitation bias ~30%).

This tropical overestimation persists for mean runoff in MIROC/MIROC5 and, to a lesser extent, in CCCma/CanAM4 when compared with observed river flow data obtained from the World Meteorological Organization Global Runoff Data Center, GRDC (Fekete *et al* 2002). ETH/CAM4-2degree and NCC/NorESM1-HAPPI on the other hand, show an importantly reduced runoff in the tropics compared with the other two AGCMs. In contrast, extra-tropical overestimation of precipitation in MIROC/MIROC5 does not lead to equally overestimated runoff in those regions. It is therefore not possible to identify the root cause for biases in river flow with confidence, given the substantial discrepancies in the precipitation-to-runoff ratio in the models. However, the fact that the two models with lowest zonal average runoff also show the lowest river flow is indicative that the treatment of the water budget and the associated hydrological balance in the AGCMs is crucial in capturing the magnitude of the river flow. That said, we emphasize that biases in river flow are unlikely to affect the change in frequency of the return time between the different temperature scenarios. This is also shown in our sampling uncertainty estimates derived from resampling our dataset 1000 times for the ten largest catchments globally (see table 1).

3.3. Magnitude of projected changes in the 100 year river flow

In contrast to the important increase in high flow occurrences, described above, we lastly find a diverse response in the change of flow magnitudes between the two temperature scenarios for the ten largest catchments in the world (see table 1). In catchments where we do not detect a large change in the frequency of occurrence of the historical 1-in-100 years return period flow such as the Amazon and Murray-Darling, we find a reduction of up to 5% in mean annual river flow under the 1.5 °C scenario. In contrast, some mean river flows such as those at the outlets of northern catchments (Mackenzie and Ob') show important increases of up to 8% (at 2.0 °C) despite quasi-constant changes in frequency of occurrence of peak flows. At the Yangtze river, apart from the increase in the frequency of occurrence of extreme river-flows as presented above, there is an important increase in the mean discharge at both, 1.5 °C–2.0 °C. Also, we note that for the Mississippi and the Ganges rivers the small change in mean river flow is contrasted by an important increase in high flow frequencies. Also, we note that regarding flow magnitude, the change from 1.5 °C to 2.0 °C levels of warming are not as clear as those detected for high river flow frequencies. However, we note that the combined fidelity of the

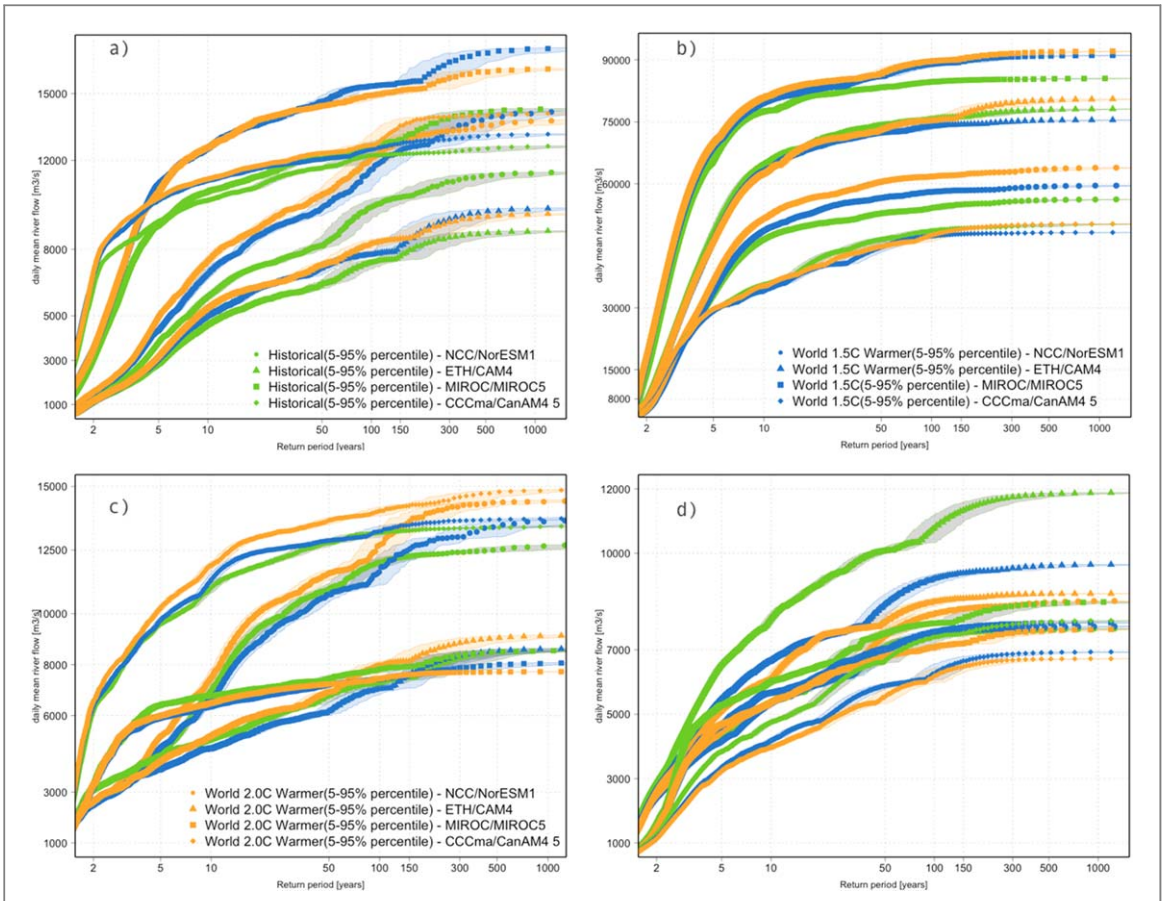

Figure 4. Maximum one-day river flow as simulated by the four AGCMs ensemble (a) the outlet area of Yangtze River, (b) outlet of the Ganges River, (c) the upper Blue Nile (Ethiopian Highlands), and (d) the Orange River in South Africa.

ensemble of our AGCMs and the river routing model to reproduce the annual cycle of the river flow, exemplified for a subset of major river catchments is limited in certain areas (see supplementary figure 5). The representation of the water budget and hydrological balance discussed in the section above may also be affecting the ability to represent changes in flow magnitudes.

3.4. Flow responses for alternative return periods

We note that although the four AGCMs ensemble disagree in maximum daily flow magnitudes, they are not sensitive to the choice of the return time as highlighted in figure 4, where we have plotted the return times for all scenarios and models for four different rivers which are affecting a large fraction of global population. At the Yangtze as well as at the Orange outlets, we find that the difference between 1.5 °C and 2.0 °C remains small for a wide range of return times (figures 4(a)/(d)). As mentioned above, the four models show similar tendencies when simulating changes in return periods of high flows for the selected regions, which suggests that our flow frequency results are indeed robust, despite biases in the magnitude of the river flow. The detected wet bias in runoff at certain latitudes in MIROC/MIROC5 reappears here, in that we find the river flow magnitude to be overestimated at the Yangtze and the Ganges (figures 4(a), (b)). Also, the difference in runoff between the two wettest and driest AGCMs is mirrored in the return time plots at the Upper Blue Nile (figure 4(c)), where we find considerably higher river flow magnitudes between the two model subsets. In other words, the regionally-overestimated precipitation (~30% in NCC/NorESM1-HAPPI and CCCma/CanAM4) translates directly into higher mean and extreme river flows.

4. Discussion

The results shown here agree with various of the previous findings that also project shifts in runoff, river flow magnitudes and flood frequencies under representative concentration pathways in various global regions (Hirabayashi *et al* 2013, Stocker *et al* 2013, Dankers *et al* 2014, Koirala *et al* 2014, Schewe *et al* 2014, Arnell and Gosling 2016). For instance, our findings consistently agree with the projection of increased mean river flows and high flow frequencies for Southeast Asia, eastern Africa, and various parts of South America. Similarly, for a world 1.5 °C and 2.0 °C warmer, Döll *et al* (2018) also project increases in high flows in South and South Asia, and Central Africa. On the contrary, these studies typically

suggest a general decrease in future high flows in central-eastern Europe. On the contrary, our results project an increase in high flow frequencies in this region (relatively good multi-model consistencies found here).

Also, the nonlinearity found between current conditions and the two future warming scenarios might as well be related to counterbalancing effects due to the presence of different forcing agents that vary greatly over time. In both HAPPI future scenarios, the aerosol load is reduced to approximately one third of its current levels. This leads many regions to show higher rainfall increases at 1.5 °C compared to what has been observed or simulated in similar experiments as high aerosol loads have been connected to a reduced strength of the hydrological cycle in several global regions (Bollasina *et al* 2011). This may be the case in the Asian monsoon region which is generally characterized with high aerosol loads and our results show an increase in high flow frequencies detected here. If the role these different drivers are playing is not appropriately analyzed, the attribution results can easily be misinterpreted. As such, it is also important to understand other region-specific features which may explain the different local flow responses between both scenarios.

Moreover, the consistent decrease in high flow frequencies found in our study for Scandinavia and South Africa has been previously estimated by Hirabayashi *et al* (2013) and Koirala *et al* (2014) for the RCP8.5 scenario. Similar projections were also found by Döll *et al* (2018) for the particular temperature targets agreed in Paris. Also, it is important to note that in some areas where consistently project an increase in high flow frequencies, various previous reports estimate a future decrease in mean river flow accompanied by major drought hazard at 2.0 °C (Schewe *et al* 2014, Lehner *et al* 2017). These areas include, southern China (such as the Yangtze river), central Europe, and central South America. Thus, our findings suggest an intensification of hydrological extremes in these regions. Yet it is important to consider the additional role that that the reduction of aerosols, described previously, may have in showing wetter futures in our estimates in these regions.

5. Conclusions

By using the HAPPI Protocol, which is a framework designed to reduce the influence of model sensitivity in climate outputs, we analyze the impacts of an additional half degree of warming on high river flows, as agreed in Paris in 2015. We find that historical extreme flows (represented by 1-in-100 year return periods) occur more frequently at 1.5 °C, but even greater additional changes are projected for many regions at 2.0 °C. These regions include most of South America, central Africa, central-western Europe, the south of the US (Mississippi river area), central Asia, and Siberian catchments. We detect that in these regions, the median increase of the frequency of the current 1-in-100 year flow is once in 70–90 years at 1.5 °C, and at 2.0 °C this frequency increases to at least once in 50 years. Our result suggests that in these areas (with the exception of Siberia), this change is accompanied by shorter, and consequently more intense, rainy seasons. As such, committing to a 1.5 °C level of warming reduces the chance of high flows in these regions. In other highly populated areas, such as South and Southeast Asia (south of the Yangtze river) and the Indus river basin, the current 1-in-100 year becomes more frequent at a 1.5 °C level of warming (1-in-50 year). Then the change from 1.5 °C to 2.0 °C is not importantly appreciable. Yet it is important to note that reductions in atmospheric aerosol loading represented in the HAPPI experiments lead to wetter futures in the areas discussed. As such, the implications that regional-scale processes may have in our results may be worth noting in a context of global mitigation targets. Lastly, while our analysis highlights limitations concerning regional and seasonal river flow projections produced using global models, we have demonstrated that our river flow results are robust with regard to changing risks tendencies. Thus, our results may be used to inform adaptation strategies and to guide assessments of socio-economic impacts at the regional or catchment scale.

ORCID iDs

Homero Paltan https://orcid.org/0000-0001-6952-6850

References

Alfieri L *et al* 2017 Global projections of river flood risk in a warmer world *Earth's Future* **5** 171–82

Arnell N W and Gosling S N 2016 The impacts of climate change on river flood risk at the global scale *Clim. Change* **134** 387–401

Arnell N W and Lloyd-Hughes B 2014 The global-scale impacts of climate change on water resources and flooding under new climate and socio-economic scenarios *Clim. Change* **122** 127–40

Becker A 2011 *GPCC full data reanalysis version 7.0 at 0.5: Monthly land-surface precipitation from rain-gauges built on GTS-based and historic data* (https://doi.org/10.5676/DWD_GPCC/FD_M_V6_050)

Bell V A *et al* 2007 Development of a high resolution grid-based river flow model for use with regional climate model output *Hydrol. Earth Syst. Sci.* **11** 532–49

Beven K J 2012 *Rainfall-Runoff Modelling: The Primer* (New York: Wiley) (https://doi.org/10.1002/9781119951001)

Bollasina M A, Ming Y and Ramaswamy V 2011 Anthropogenic aerosols and the weakening of the South Asian summer monsoon *Science* **334** 502LP–5

Clark D B and Gedney N 2008 Representing the effects of subgrid variability of soil moisture on runoff generation in a land surface model *J. Geophys. Res.* **113** D10111

Dadson S J, Bell V A and Jones R G 2011 Evaluation of a grid-based river flow model configured for use in a regional climate model *J. Hydrol.* **411** 238–50

Dankers R and Feyen L 2008 Climate change impact on flood hazard in Europe: an assessment based on high-resolution climate simulations *J. Geophys. Res. Atmos.* **113** 1–17
Dankers R *et al* 2014 First look at changes in flood hazard in the Inter-Sectoral Impact Model Intercomparison Project ensemble *Proc. Natl Acad. Sci.* **111** 3257–61
Davies H N and Bell V A 2009 Assessment of methods for extracting low-resolution river networks from high-resolution digital data *Hydrol. Sci. J.—J. Sci. Hydrologiques* **54** 17–28
Döll P *et al* 2018 Risks for the global freshwater system at 1.5 °C and 2 °C global warming *Environ. Res. Lett.* **13** 44038
Fekete B, Vörösmarty C and W G 2002 *Global Composite Runoff Fields on Observed River Discharge and Simulated Water Balances* (Koblenz, Germany: Water System Analysis Group, University of New Hampshire, and Global Runoff Data Centre)
Gash J H C 1979 An analytical model of rainfall interception by forests *Q. J. R. Meteorol. Soc.* **105** 43–55
Gumbel E J 1941 The return period of flood flows *Ann. Math. Stat.* **12** 163–90
Hirabayashi Y *et al* 2008 Global projections of changing risks of floods and droughts in a changing climate *Hydrol. Sci. J.* **53** 754–72
Hirabayashi Y *et al* 2013 Global flood risk under climate change *Nat. Clim. Change* **3** 816–21
Hock R 2003 Temperature index melt modelling in mountain areas *J. Hydrol.* **282** 104–15
Hosking J R M and Wallis J R 2005 *Regional Frequency Analysis: An Approach Based on L-Moments* (Cambridge: Cambridge University Press)
Hulme M 2016 1.5 °C and climate research after the Paris Agreement *Nat. Clim. Change* **6** 222–4
Jongman B *et al* 2014 Increasing stress on disaster-risk finance due to large floods *Nature Clim. Change* **4** 1–5
Koirala S *et al* 2014 Global assessment of agreement among stream flow projections using CMIP5 model outputs *Environ. Res. Lett.* **9** 64017
Lehner F *et al* 2017 Projected drought risk in 1.5 °C and 2 °C warmer climates *Geophys. Res. Lett.* **44** 7419–28
Materia S *et al* 2009 The sensitivity of simulated river discharge to land surface representation and meteorological forcings *J. Hydrometeorol.* **11** 334–51
Milly P C D *et al* 2002 Increasing risk of great floods in a changing climate *Nature* **415** 514–7
Mitchell D *et al* 2016 Realizing the impacts of a 1.5 °C warmer world *Nat. Clim. Change* **6** 735–7
Mitchell D *et al* 2017 Half a degree additional warming, prognosis and projected impacts (HAPPI): background and experimental design *Geosci. Model Dev. Discuss.* 571–83
Monteith J L 1965 *Evaporation and environment Symp. Soc. Exp. Biol* 19 (Cambridge) 205–23
Moore R J *et al* 1999 Methods for snowmelt forecasting in upland Britain *Hydrol. Earth Syst. Sci. Discuss.* **3** 233–46
Nijssen B *et al* 2001 Hydrologic sensitivity of global rivers to climate change *Clim. Change* **50** 143–75
Okazaki A, Yeh P J F, Yoshimura K, Watanabe M, Kimoto M and Oki T 2012 Changes in flood risk under global warming estimated using MIROC5 and the discharge probability index *J. Meteorolog. Soc. Jpn. Ser. II* **90** 509–24
Oki T and Sud Y C 1998 Design of total runoff integrating pathways (TRIP)—a global river channel network *Earth Interact.* **2** 1–37
Olivera F and Raina R 2003 Development of large scale gridded river networks from vector stream data *J. Am. Water Resour. Assoc.* **39** 1235–48
Parajka J *et al* 2010 Evaluation of snow cover and depth simulated by a land surface model using detailed regional snow observations from Austria *J. Geophys. Res.* **115** D24117
Peduzzi P *et al* 2009 Assessing global exposure and vulnerability towards natural hazards: the disaster risk index *Nat. Hazards Earth Syst. Sci.* **9** 1149–59
Qian T *et al* 2006 Simulation of global land surface conditions from 1948 to 2004: I. Forcing data and evaluations *J. Hydrometeorol.* **7** 953–75
Qiaohong S *et al* 2017 A review of global precipitation data sets: data sources, estimation, and intercomparisons *Rev. Geophys.* **56** 79–107
Rango A and Martinec J 2007 Revisiting the degree day-method for snowmleat computations *JAWRA J. Am. Water Resour. Assoc.* **31** 657–69
Rogelj J *et al* 2016 Perspective : Paris Agreement climate proposals need boost to keep warming well below 2 °C *Nat. Clim. Change* **534** 631–9
Schellnhuber H J, Rahmstorf S and Winkelmann R 2016 Why the right climate target was agreed in Paris *Nature Clim. Change* **6** 649–53
Schewe J *et al* 2014 Multimodel assessment of water scarcity under climate change *Proc. Natl Acad. Sci.* **111** 3245LP–50
Stocker T F *et al* 2013 Technical summary *Climate change 2013: The Physical Science Basis. Contribution of Working Group I to the Fifth Assessment Report of the Intergovernmental Panel on Climate Change.* (Cambridge: Cambridge University Press) pp 33–115
Ukkola A M and Prentice I C 2013 A worldwide analysis of trends in water-balance evapotranspiration *Hydrol. Earth Syst. Sci. Discuss.* **10** 4177–87
Wake B 2013 Flooding costs *Nature* **3** 778
Ward P *et al* 2013 Assessing flood risk at the global scale: model setup, results, and sensitivity *Environ. Res. Lett.* **8** 44019
Winsemius H C *et al* 2015 Global drivers of future river flood risk *Nature Clim. Change* **6** 381
Zhang Y, Liu S and Ding Y 2006 Observed degree-day factors and their spatial variation on glaciers in western China *Ann. Glaciol.* **43** 301–6